

e^+e^- annihilation to $\pi^0\pi^0\gamma$ and $\pi^0\eta\gamma$ as a source of information on scalar and vector mesons

S. Eidelman^{1,2}, S. Ivashyn^{3,4}, A. Korchin³, G. Pancheri⁵ and O. Shekhovtsova^{3,5}

¹ Budker Institute of Nuclear Physics, Novosibirsk, Russia

² Novosibirsk State University, Novosibirsk, Russia

³ Institute for Theoretical Physics, NSC “Kharkov Institute of Physics and Technology”, UA-61108 Kharkov, Ukraine

⁴ Institute of Physics, University of Silesia, PL-40007 Katowice, Poland

⁵ INFN LNF, Frascati (RM) 00044, Italy

e-mail: simon.eidelman@cern.ch, ivashin.s@rambler.ru,

korchin@kipt.kharkov.ua, giulia.pancheri@lnf.infn.it, shekhovtsova@kipt.kharkov.ua

July 08, 2010

Abstract We present a general framework for the model-independent decomposition of the fully differential cross section of the reactions $e^+e^- \rightarrow \gamma^* \rightarrow \pi^0\pi^0\gamma$ and $e^+e^- \rightarrow \gamma^* \rightarrow \pi^0\eta\gamma$, which can provide important information on the properties of scalar mesons: $f_0(600)$, $f_0(980)$ and $a_0(980)$. For the model-dependent ingredients in the differential cross section, an approach is developed, which relies on Resonance Chiral Theory with vector and scalar mesons. Numerical results are compared to data. The framework is convenient for development of a Monte Carlo generator and can also be applied to the reaction $e^+e^- \rightarrow \gamma^* \rightarrow \pi^+\pi^-\gamma$.

1 Introduction

Despite extensive studies during last decades, physics of the light scalar mesons $a_0(980)$ ($I^G(J^{PC}) = 1^-(0^{++})$), $f_0(980)$ and $f_0(600) \equiv \sigma$ ($I^G(J^{PC}) = 0^+(0^{++})$) is far from complete understanding. In particular, there are doubts whether simple quark model can explain their properties, see, e.g., the review in [1].

The dominant decay channels of scalar mesons are known to be $\pi^+\pi^-$, $\pi^0\pi^0$ for the $f_0(980)$ and σ meson, and $\pi^0\eta$ for the $a_0(980)$ meson. Much experimental attention has already been paid to the radiative decays of the ϕ meson: $\phi(1020) \rightarrow \gamma a_0 \rightarrow \gamma\pi\eta$ [2,3] and $\phi(1020) \rightarrow \gamma f_0$ (or $\gamma\sigma) \rightarrow \gamma\pi\pi$ [4,5] (see also the KLOE summary in [6] and results from Novosibirsk [7,8,9]). Such measurements are a good source of information about the scalar meson properties [10]. Various models have been proposed to describe these decays, [10,11,12,13,14], to mention a few. The calculated decay widths turn out to be very sensitive to model ingredients, however, the experimental data is still insufficient to unambiguously discriminate between the models.

In the case of the neutral final state (FS), i.e., $\pi^0\pi^0\gamma$ and $\pi^0\eta\gamma$, the cross section is determined solely by final-state radiation (FSR) mechanism, since there is no initial-state radiation (ISR) contribution resulting in the same final state. Despite the lower value of the cross section, compared to the charged pion case ($e^+e^- \rightarrow \pi^+\pi^-\gamma$), processes with the neutral-meson FS are an invaluable source of information on complicated hadron dynamics.

In this paper we describe the differential cross section of the e^+e^- annihilation to a pair of neutral pseudoscalar mesons and one photon in the FS,

$$e^+(p_+) e^-(p_-) \rightarrow \gamma^* \rightarrow P_1(p_1) P_2(p_2) \gamma(k). \quad (1)$$

The pseudoscalar mesons ($J^{PC} = 0^{-+}$) are denoted by $P_1P_2 \equiv \pi^0\pi^0$ and $\pi^0\eta$. In Section 2 we present a formalism for a differential cross section, which is the main task of this paper. We provide more general formulae in comparison with Refs. [15,16,17], namely, the non-integrated expressions are given as well as those integrated over the angles. It gives a convenient ground to implement the results in the Monte Carlo generators, e.g., in FASTERD [18] (based on the general structure given in Ref. [15]) or PHOKHARA [19].

Our framework is consistent with symmetries of the strong and electromagnetic interactions. It incorporates a model-dependent description of the FSR only through the explicit form of the Lorentz-invariant functions $f_{1,2,3}$ and has a model-independent tensor decomposition.

In Sections 3 and 4 we calculate the FS hadronic tensor. It is the second goal of the paper to provide such a description in terms of functions $f_{1,2,3}$. Our model relies on the Lagrangian of Resonance Chiral Theory (R χ T) [20]. The R χ T is a consistent extension of Chiral Perturbation Theory to the region of energies near 1 GeV, which introduces the explicit resonance fields and exploits the idea of resonance saturation. One of the advantages of the R χ T Lagrangian at leading order (LO), which makes it convenient for the present study, is that, having a good

predictive power, it contains very few free parameters compared with other phenomenological models. In order to get good agreement with data, we release a rigor of $R\chi T$ and include some $SU(3)$ symmetry breaking effects (e.g., use realistic masses of vector mesons) and mixing phenomena (e.g., a G-parity-violating $\phi\omega\pi^0$ transition).

The loop contributions follow from the model Lagrangian. For example, the kaon loop in the $\phi f_0\gamma$ transition, which is often considered as a pure phenomenology manifestation, in the present model is a direct consequence of the $R\chi T$ Lagrangian. In order to simplify the formulae, some numerically irrelevant loop contributions are omitted. In addition, the resonance exchanges in the loops are not considered to avoid problems with renormalizability.

We consider in detail the following intermediate states with scalar and vector resonances, which lead to the same FS $P_1P_2\gamma$:

$$\begin{aligned} & \text{scalar decay, (Section 3)} \\ e^+e^- & \rightarrow \gamma^* \rightarrow S\gamma \rightarrow P_1P_2\gamma & (2) \\ e^+e^- & \rightarrow \gamma^* \rightarrow V \rightarrow S\gamma \rightarrow P_1P_2\gamma \\ & \text{vector contribution, (Section 4)} \\ e^+e^- & \rightarrow \gamma^* \rightarrow VP_{1,2} \rightarrow P_1P_2\gamma & (3) \\ e^+e^- & \rightarrow \gamma^* \rightarrow V_a \rightarrow V_bP_{1,2} \rightarrow P_1P_2\gamma \end{aligned}$$

where S ($J^{PC} = 0^{++}$) is an intermediate scalar meson ($S = f_0, \sigma$ for $\pi_0\pi_0$ FS and $S = a_0$ for $\pi_0\eta$). Only the lowest nonet of vector mesons ($V, V_a, V_b = \rho, \omega$ and ϕ) is taken into account.

We are interested in the center-of-mass energy \sqrt{s} range from the threshold up to M_ϕ . This framework may also be used in a somewhat dedicated case of $\sqrt{s} = M_\phi$, giving, e.g., the ϕ radiative decay description.

For the quantitative illustration of our approach, in Section 5 we show the numerical results for the values of $\sqrt{s} = 1$ GeV and $\sqrt{s} = M_\phi$. The meson-pair invariant mass distributions are of interest, and for $\sqrt{s} = M_\phi$ they are compared with available results from KLOE. We demonstrate the interplay of the contributions (2) and (3). Conclusions follow in Section 6.

2 General structure of the FSR cross section

For a generic reaction $e^+e^- \rightarrow \gamma P_1P_2$ we define 4-momenta as shown in Fig. 1:

$$\begin{aligned} p &= p_+ + p_-, & l &= p_+ - p_-, & (4) \\ Q &= p_+ + p_- = k + p_1 + p_2. \end{aligned}$$

The masses of pseudoscalars are $m(P_1) = m_1, m(P_2) = m_2$.

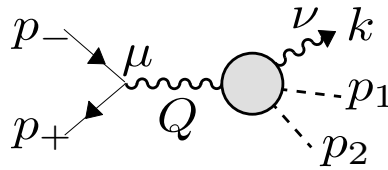


Figure 1. Generic scheme for electron-positron annihilation into two particles with final state radiation

The cross section of the FSR process can be written as

$$\begin{aligned} d\sigma_F &= \frac{1}{2s(2\pi)^5} C_{12} \\ & \times \int \delta^4(Q - p_1 - p_2 - k) |M_{FSR}|^2 \frac{d^3p_1 d^3p_2 d^3k}{8E_1E_2\omega} \\ &= C_{12} N \int |\overline{M_{FSR}}|^2 d\cos\theta d\phi dm_{1\gamma}^2 dp^2, & (5) \\ N &= \frac{1}{(2\pi)^4} \frac{1}{64s^2}, \end{aligned}$$

where $s = Q^2, \theta$ is the azimuthal angle, ϕ is the polar angle of the photon and $m_{1\gamma}^2 = (k + p_1)^2$. The factor $C_{12} = 1/2$ for $\pi^0\pi^0$ in the final state and $C_{12} = 1$ for $\pi^0\eta$. The matrix element M_{FSR} is

$$M_{FSR} = \frac{e}{s} M^{\mu\nu} \bar{u}(-p_+) \gamma_\mu u(p_-) \epsilon_\nu^*, & (6)$$

where $e = \sqrt{4\pi\alpha} \approx \sqrt{4\pi/137} \approx 0.303$ and the FSR tensor $M^{\mu\nu}$ can be decomposed into three gauge-invariant independent tensors:

$$\begin{aligned} M^{\mu\nu}(Q, k, l) &\equiv -ie^2(\tau_1^{\mu\nu} f_1 + \tau_2^{\mu\nu} f_2 + \tau_3^{\mu\nu} f_3), & (7) \\ \tau_1^{\mu\nu} &= k^\mu Q^\nu - g^{\mu\nu} k \cdot Q, \\ \tau_2^{\mu\nu} &= k \cdot l (l^\mu Q^\nu - g^{\mu\nu} Q \cdot l) + l^\nu (k^\mu Q \cdot l - l^\mu k \cdot Q), \\ \tau_3^{\mu\nu} &= Q^2 (g^{\mu\nu} k \cdot l - k^\mu l^\nu) + Q^\mu (l^\nu k \cdot Q - Q^\nu k \cdot l) \end{aligned}$$

with the Lorentz-invariant functions

$$f_i \equiv f_i(Q^2, k \cdot Q, k \cdot l), & (8)$$

$i = 1, 2, 3$. If $m_1 = m_2$, these tensors coincide with those of Ref. [15, 21]. One may also find a similar approach in [17, 22, 23]. We emphasize that the decomposition (7) is model independent; the model dependence is contained in an explicit form of functions f_i only. Notice that the scalar products can be written in terms of the invariant masses:

$$\begin{aligned} k \cdot Q &= (s - p^2)/2, \\ k \cdot l &= m_{1\gamma}^2 - m_1^2 - k \cdot Q, \\ Q \cdot l &= k \cdot l + s\delta/2, & (9) \end{aligned}$$

where $\delta \equiv 2(m_1^2 - m_2^2)/s$.

For the matrix element squared and averaged over the e^+e^- polarizations we obtain

$$\begin{aligned} \overline{|M_{FSR}|^2} &= \frac{e^6}{s^2} \left[a_{11} |f_1|^2 + 2a_{12} \text{Re}(f_1 f_2^*) + a_{22} |f_2|^2 \right. \\ & \left. + 2a_{23} \text{Re}(f_2 f_3^*) + a_{33} |f_3|^2 + 2a_{13} \text{Re}(f_1 f_3^*) \right], & (10) \end{aligned}$$

with the coefficients

$$a_{ik} \equiv \left(\frac{s}{2} g_{\mu\rho} - p_{+\mu} p_{-\rho} - p_{+\rho} p_{-\mu} \right) \tau_i^{\mu\nu} \tau_k^{\rho\lambda} g_{\nu\lambda}, \quad (11)$$

equal to

$$\begin{aligned} a_{11} &= \frac{1}{4} s (t_1^2 + t_2^2), \\ a_{22} &= \frac{1}{8} \left[sl^4 (t_1 + t_2)^2 + 4l^2 (u_1^2 (s^2 + s(t_1 + t_2) + t_2^2) \right. \\ &\quad \left. + u_2^2 (s^2 + s(t_1 + t_2) + t_1^2) \right. \\ &\quad \left. + 2u_1 u_2 (s^2 + s(t_1 + t_2) - t_1 t_2) \right. \\ &\quad \left. + 8s (u_1^2 + u_2^2) (u_1 + u_2)^2 \right] \\ &\quad - (4u_1^2 + 4u_2^2 + l^2 (2s + t_1 + t_2)) \frac{s^2 (u_1 + u_2) \delta}{4} \\ &\quad + (l^2 s + 2u_1^2 + 2u_2^2) \frac{s^3 \delta^2}{8}, \\ a_{33} &= -\frac{s^2}{2} (t_1 t_2 l^2 + 2(u_1 + u_2) (u_2 t_1 + u_1 t_2) \\ &\quad - \delta s (u_2 t_1 + u_1 t_2)), \\ a_{12} &= \frac{1}{8} \left[sl^2 (t_1 + t_2)^2 + 4u_1^2 (s^2 + st_2 + t_2^2) \right. \\ &\quad \left. + 4u_2^2 (s^2 + st_1 + t_1^2) + 4u_1 u_2 (2s^2 + s(t_1 + t_2) - 2t_1 t_2) \right. \\ &\quad \left. + 2s^2 (t_1 u_2 + t_2 u_1 + 2s(u_1 + u_2)) \delta + s^4 \delta^2 \right], \\ a_{13} &= \frac{s}{4} \left[(u_1 + u_2) (st_1 + st_2 + t_1 t_2) - u_1 t_2^2 - u_2 t_1^2 \right. \\ &\quad \left. - \frac{\delta}{2} (t_1 + t_2) s^2 \right], \\ a_{23} &= \frac{s}{4} \left[l^2 (u_1 t_2 - u_2 t_1) (t_1 - t_2) - 2s (u_1 + u_2)^3 \right. \\ &\quad \left. + 2(u_1 + u_2) (u_1 - u_2) (t_2 u_1 - u_2 t_1) \right. \\ &\quad \left. + \delta s (u_1 u_2 (4s + t_1 + t_2) + u_1^2 (2s - t_2) + u_2^2 (2s - t_2)) \right. \\ &\quad \left. - \frac{\delta^2}{2} s^3 (u_1 + u_2) \right], \end{aligned} \quad (12)$$

where

$$\begin{aligned} t_1 &\equiv (p_- - k)^2 - m_e^2 = -2p_- \cdot k, \\ t_2 &\equiv (p_+ - k)^2 - m_e^2 = -2p_+ \cdot k, \\ u_1 &\equiv l \cdot p_-, \quad u_2 \equiv l \cdot p_+. \end{aligned} \quad (13)$$

For numerical calculations the relation $l^2 = 2(m_1^2 + m_2^2) - p^2$ may be useful.

The Eqs. (5) and (10), with the explicit expressions (12) and (13), fix the whole model-independent part of the differential cross section. It is worth illustrating a relation of these formulae to the partial differential cross section. Taking into account the corresponding factors and integrating the coefficients a_{ik} over the angular variables

of the final-meson phase space we have

$$\begin{aligned} \frac{d\sigma}{dm_{1\gamma}^2 dp^2} &= \frac{\alpha^3 C_{12}}{32s} (A_{11} |f_1|^2 + 2A_{12} \text{Re}(f_1 f_2^*) + A_{22} |f_2|^2 \\ &\quad + 2A_{23} \text{Re}(f_2 f_3^*) + A_{33} |f_3|^2 + 2A_{13} \text{Re}(f_1 f_3^*)), \end{aligned} \quad (14)$$

where

$$\begin{aligned} A_{11} &= \frac{4x^2}{3}, \\ A_{12} &= \frac{2s}{3} [(x_1 - x_2)^2 + x^2(\sigma - 1 + x) - 2\delta(x_1 - x_2) + \delta^2], \\ A_{13} &= -\frac{4s}{3} x(x_1 - x_2 - \delta) \\ A_{23} &= -\frac{2s^2}{3} (x_1 - x_2)(\delta - x_1 + x_2)^2, \\ A_{22} &= \frac{s^2}{3} [(x_1 - x_2)^4 + 2(x_1 - x_2)^2(1 - x)(\sigma - 1 + x) \\ &\quad + 2x^2(\sigma - 1 + x)^2 \\ &\quad - 2\delta(x_1 - x_2)((x_1 - x_2)^2 + (\sigma - 1 + x)(x_1 + x_2)) \\ &\quad + \delta^2((x_1 - x_2)^2 + 2(\sigma - 1 + x))], \\ A_{33} &= \frac{2s^2}{3} [(x_1 - x_2)^2(1 + x) - x^2(\sigma - 1 + x) \\ &\quad + \delta(\delta - (2 + x)(x_1 - x_2))], \end{aligned} \quad (15)$$

and

$$\begin{aligned} x &= \frac{s - p^2}{s}, \quad x_1 = \frac{2E_1}{\sqrt{s}} = \frac{p^2 + m_{1\gamma}^2 - m_2^2}{s}, \\ x_2 &= \frac{2E_2}{\sqrt{s}} = \frac{s + m_2^2 - m_{1\gamma}^2}{s}, \quad \sigma = \frac{2(m_1^2 + m_2^2)}{s}. \end{aligned} \quad (16)$$

For the case $m_1 = m_2$ Eq. (12) reduces to Eq. (17) of Ref. [15]. Also the results (14), (15) coincide with Eqs. (2.7), (2.8) of [16]. However, for an MC generator, the expressions (5) and (10) with coefficients a_{ik} are more convenient than (14).

Integrating Eq. (14) over $m_{1\gamma}^2$ one obtains the distribution of the invariant mass $\sqrt{p^2}$ of two pseudoscalar mesons:

$$\frac{d\sigma}{d\sqrt{p^2}} = 2\sqrt{p^2} \int_{(m_{1\gamma}^2)_{min}}^{(m_{1\gamma}^2)_{max}} dm_{1\gamma} \left(\frac{d\sigma}{dm_{1\gamma} dp^2} \right). \quad (17)$$

The bounds of integration over $m_{1\gamma}^2$ at the fixed value of p^2 are determined by

$$\begin{aligned} (m_{1\gamma}^2)_{max/min} &= \frac{s(p^2\sigma + s\delta)}{4p^2} \\ &\quad + \frac{s - p^2}{2} \left(1 \pm \sqrt{1 - \frac{s\sigma}{p^2} + \frac{s^2\delta^2}{4p^4}} \right) \end{aligned} \quad (18)$$

At the ϕ -meson peak ($s = M_\phi^2$) one can present the results in terms of the branching ratio for the $\phi \rightarrow P_1 P_2 \gamma$

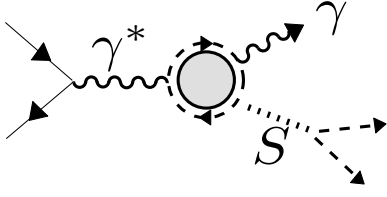


Figure 2. Scheme of $e^+e^- \rightarrow S\gamma \rightarrow P_1P_2\gamma$ subprocess

decay, which is related to the cross section as follows:

$$\frac{dB(\phi \rightarrow P_1P_2\gamma)}{d\sqrt{p^2}} = \frac{M_\phi^2}{12\pi B(\phi \rightarrow e^+e^-)} \times \frac{d\sigma(e^+e^- \rightarrow P_1P_2\gamma)}{d\sqrt{p^2}}, \quad (19)$$

where the $\phi \rightarrow e^+e^-$ branching ratio $B(\phi \rightarrow e^+e^-)$ is used. In the context of this paper, a calculation of this branching ratio is useful for comparison of model predictions with available data.

3 Scalar contribution

In this Section we consider in detail the transition amplitudes

$$\begin{aligned} \gamma^* &\rightarrow f_0\gamma \rightarrow \pi^0\pi^0\gamma, \\ \gamma^* &\rightarrow \sigma\gamma \rightarrow \pi^0\pi^0\gamma, \\ \gamma^* &\rightarrow a_0\gamma \rightarrow \pi^0\eta\gamma \end{aligned} \quad (20)$$

for the $\pi^0\pi^0\gamma$ and $\pi^0\eta\gamma$ final states, respectively. They contribute to $e^+e^- \rightarrow S\gamma \rightarrow P_1P_2\gamma$ as illustrated in Fig. 2. To describe the processes (20) we use the Lagrangian of $R\chi T$ [20] at the linear-in-resonance level, following [12, 24]. The basic features of the Lagrangian framework of the $R\chi T$ are sketched in Appendix A. We emphasize that both light isoscalar scalar resonances, f_0 and σ are included in the formalism in a natural way. Throughout this section we work in the tensor representation for spin-1 particles [20, 25]. In the present work we take into account the pseudoscalar decay constants splitting ($f_\pi \neq f_K$) which was discussed in the same context in Ref. [24].

The interaction of pseudoscalars with the photon field B^μ in $R\chi T$ is identical to the scalar QED. We shall now discuss the interaction terms of the Lagrangian (A3) relevant to the processes (20) (cf. [12]). For the vector mesons in the even-intrinsic-parity sector one has

$$\mathcal{L}_{\gamma V} = eF_V F^{\mu\nu} \left(\frac{1}{2}\rho_{\mu\nu}^0 + \frac{1}{6}\omega_{\mu\nu} - \frac{1}{3\sqrt{2}}\phi_{\mu\nu} \right), \quad (21)$$

$$\begin{aligned} \mathcal{L}_{VPP} = & iG_V \left[\frac{1}{f_\pi^2} (2\rho_{\mu\nu}^0 \partial^\mu \pi^+ \partial^\nu \pi^-) \right. \\ & + \frac{1}{f_K^2} (\rho_{\mu\nu}^0 + \omega_{\mu\nu} - \sqrt{2}\phi_{\mu\nu}) (\partial^\mu K^+ \partial^\nu K^-) \\ & \left. + \frac{1}{f_K^2} (-\rho_{\mu\nu}^0 + \omega_{\mu\nu} - \sqrt{2}\phi_{\mu\nu}) (\partial^\mu K^0 \partial^\nu \bar{K}^0) \right], \quad (22) \end{aligned}$$

$$\begin{aligned} \mathcal{L}_{\gamma VPP} = & -\frac{eF_V}{f_\pi^2} \partial^\mu B^\nu \rho_{\mu\nu}^0 \pi^+ \pi^- \\ & -\frac{eF_V}{2f_K^2} \partial^\mu B^\nu (\rho_{\mu\nu}^0 + \omega_{\mu\nu} - \sqrt{2}\phi_{\mu\nu}) K^+ K^- \\ & -\frac{2eG_V}{f_\pi^2} B^\nu \rho_{\mu\nu}^0 (\pi^+ \partial^\mu \pi^- + \pi^- \partial^\mu \pi^+) \\ & -\frac{eG_V}{f_K^2} B^\nu (\rho_{\mu\nu}^0 + \omega_{\mu\nu} - \sqrt{2}\phi_{\mu\nu}) \\ & \times (K^+ \partial^\mu K^- + K^- \partial^\mu K^+), \quad (23) \end{aligned}$$

where $F^{\alpha\beta}$ stands for the electromagnetic field tensor and $V^{\mu\nu}$ for the vector field in the tensor representation, F_V and G_V are the model parameters (see Appendix B for numerical values). Vertex functions for Eqs. (21)–(23) are shown in Table 1.

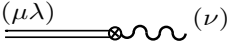
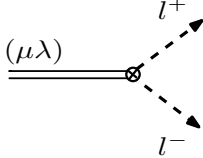
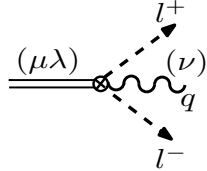
The Lagrangian terms for scalar and pseudoscalar meson interactions, which follow from (A5) are

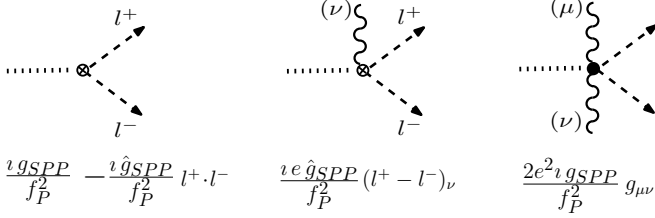
$$\begin{aligned} \mathcal{L}_{scalar} = & \sum_S S \left(\frac{1}{f_\pi^2} \frac{g_{S\pi\pi}}{2} \vec{\pi}^2 + \frac{1}{f_\pi^2} \frac{g_{S\eta\eta}}{2} \eta^2 + \frac{1}{f_\pi^2} g_{S\pi\eta} \pi^0 \eta \right. \\ & + \frac{1}{f_K^2} g_{SKK} (K^+ K^- + (-1)^{I_S} K^0 \bar{K}^0) \\ & + \frac{1}{f_\pi^2} (\hat{g}_{S\pi\pi}/2) (\partial_\mu \vec{\pi})^2 \\ & + \frac{1}{f_\pi^2} (\hat{g}_{S\eta\eta}/2) (\partial_\mu \eta)^2 + \frac{1}{f_\pi^2} \hat{g}_{S\pi^0\eta} \partial_\mu \pi^0 \partial^\mu \eta \\ & + \frac{1}{f_K^2} \hat{g}_{SKK} (\partial_\mu K^+ \partial^\mu K^- + (-1)^{I_S} \partial_\mu K^0 \partial^\mu \bar{K}^0) \\ & + \frac{1}{f_\pi^2} g_{S\gamma\pi\pi} e B_\mu \pi^+ \overleftrightarrow{\partial}_\mu \pi^- \\ & + \frac{1}{f_K^2} g_{S\gamma KK} e B_\mu K^+ \overleftrightarrow{\partial}_\mu K^- \\ & + \frac{1}{f_\pi^2} g_{S\gamma\pi\pi} e^2 B_\mu B^\mu \pi^+ \pi^- \\ & \left. + \frac{1}{f_K^2} g_{S\gamma KK} e^2 B_\mu B^\mu K^+ K^- \right). \quad (24) \end{aligned}$$

(interactions with η' are omitted here for brevity). Here S stands for any scalar field, a_0, f_0 or σ , and P – for pseudoscalar $\vec{\pi} = \pi^0, \pi^\pm$ or K^\pm, K^0, \bar{K}^0 and η . We have introduced the effective couplings $g_{S\pi\pi}, g_{S\eta\eta}$, etc. listed in Table 2, $I_S = 0$ for f_0 and σ and $I_S = 1$ for a_0 . Couplings are expressed in terms of the model parameters c_d, c_m and θ , see also the expression (A2) for the $C_{q,s}$ coefficients. The Lagrangian (24) leads to the vertices shown in Fig. 3.

Given this set of interaction terms, the leading contribution to the $\gamma^*\gamma S$ vertex comes from the one-loop diagrams [12]. The mechanism of the ϕ meson decay via the kaon loop was first considered in a different formalism in [10] and is consistent with the data [6]. We would like to stress that in the current approach the loop mechanism is a predicted subprocess following directly from the Lagrangian, rather than an assumption. In particular, for the case of the $\pi^0\pi^0\gamma$ final state both the kaon and pion loops

Table 1. The vertices from Resonance Chiral Lagrangian terms (21)–(23). The dashed line stands for pseudoscalar meson (momentum l), double solid — for vector meson, wavy line — for photon (momentum q).

Diagramm Vertex function									
	$eF_V [g_{\nu\lambda}q_\mu - g_{\nu\mu}q_\lambda]$	$\frac{G_V}{2f_P^2} [l_\mu^- l_\lambda^+ - l_\mu^+ l_\lambda^-]$	$\frac{eG_V}{2f_P^2} [g_{\nu\lambda}(l^- + l^+)_\mu - g_{\nu\mu}(l^- + l^+)_\lambda]$ $+ \frac{eF_V}{4f_P^2} [g_{\nu\lambda}q_\mu - g_{\nu\mu}q_\lambda]$	ρ	ω	ϕ	ρ	ω	ϕ
$\pi^\pm (f_P = f_\pi)$				2	0	0	2	0	0
$K^\pm (f_P = f_K)$				1	1	$-\sqrt{2}$	1	1	$-\sqrt{2}$
$K^0 (f_P = f_K)$				-1	1	$-\sqrt{2}$	0	0	0
	$\frac{1}{2}$	$\frac{1}{6}$	$\frac{-1}{3\sqrt{2}}$						

**Figure 3.** The vertices corresponding to the Lagrangian (24). The dotted line stands for a scalar meson S , the dashed one — for a pseudoscalar P . Couplings are shown in Table 2.

contribute. The latter are very important in the region of the ρ resonance (recall that the γ^* invariant mass \sqrt{s} is not constrained to the ϕ meson mass).

When working with the three-point vertex functions $\gamma^*\gamma S$, we factorize the kaon-loop part in the a_0 case and separately the pion-loop and kaon-loop part for f_0 and σ , as illustrated in Fig. 4 (see Appendix C for details). The $\gamma^*(Q^\mu) \rightarrow \gamma(k^\nu)S(p)$ amplitude reads

$$T^{\mu\nu} = -ie^2(Q^\nu k^\mu - g^{\mu\nu}Q \cdot k)F_{S\gamma^*\gamma}(p^2, Q^2). \quad (25)$$

The $\gamma^*(Q^2) \rightarrow \gamma S(p^2)$ transition form factors (FF's) have the form

$$F_{f_0\gamma^*\gamma}(p^2, Q^2) = G_{f_0\gamma^*\gamma}^{(\pi)}(p^2, Q^2) + G_{f_0\gamma^*\gamma}^{(K)}(p^2, Q^2), \quad (26)$$

$$F_{\sigma\gamma^*\gamma}(p^2, Q^2) = G_{\sigma\gamma^*\gamma}^{(\pi)}(p^2, Q^2) + G_{\sigma\gamma^*\gamma}^{(K)}(p^2, Q^2), \quad (27)$$

$$F_{a_0\gamma^*\gamma}(p^2, Q^2) = G_{a_0\gamma^*\gamma}^{(K)}(p^2, Q^2), \quad (28)$$

where the terms

$$G_{S\gamma^*\gamma}^{(\pi)}(p^2, Q^2) = \frac{G_{S\pi\pi}(p^2)}{2\pi^2 m_\pi^2} I\left(\frac{Q^2}{m_\pi^2}, \frac{p^2}{m_\pi^2}\right) F_{em}^\pi(Q^2),$$

$$G_{S\gamma^*\gamma}^{(K)}(p^2, Q^2) = \frac{G_{SKK}(p^2)}{2\pi^2 m_K^2} I\left(\frac{Q^2}{m_K^2}, \frac{p^2}{m_K^2}\right) F_{em}^K(Q^2), \quad (29)$$

for $S = f_0, \sigma$, and

$$G_{a_0\gamma^*\gamma}^{(K)}(p^2, Q^2) = \frac{G_{a_0KK}(p^2)}{2\pi^2 m_K^2} I\left(\frac{Q^2}{m_K^2}, \frac{p^2}{m_K^2}\right) F_{em}^K(Q^2) \quad (30)$$

follow from (21)–(24), and the pion and kaon electromagnetic form factors, $F_{em}^\pi(Q^2)$ and $F_{em}^K(Q^2)$, follow from (21) and (22). The terms

$$G_{SKK}(p^2) \equiv 1/f_K^2 (\hat{g}_{SKK}(m_K^2 - p^2/2) + g_{SKK}),$$

$$G_{S\pi\pi}(p^2) \equiv 1/f_\pi^2 (\hat{g}_{S\pi\pi}(m_\pi^2 - p^2/2) + g_{S\pi\pi}), \quad (31)$$

for $S = f_0, \sigma$ and

$$G_{a_0KK}(p^2) \equiv 1/f_K^2 (\hat{g}_{a_0KK}(m_K^2 - p^2/2) + g_{a_0KK}),$$

$$G_{a_0\pi\eta}(p^2) \equiv 1/f_\pi^2 (\hat{g}_{a_0\pi\eta}(m_\eta^2 + m_\pi^2 - p^2)/2 + g_{a_0\pi\eta}) \quad (32)$$

have the meaning of momentum-dependent SPP vertices. The expression for $I(a, b)$ in (29)–(30) coincides with that of [11, 14] and for convenience is given in Appendix C.

The scalar meson contribution relevant to the $\pi^0\pi^0$ final state is

$$f_1^{S, \pi^0\pi^0} = \sum_{S=f_0, \sigma} D_S(p^2) G_{S\pi\pi}(p^2) \left(G_{S\gamma^*\gamma}^{(\pi)}(p^2, Q^2) + G_{S\gamma^*\gamma}^{(K)}(p^2, Q^2) \right), \quad (33)$$

and in the $\pi^0\eta$ case one has

$$f_1^{S, \pi^0\eta} = D_{a_0}(p^2) G_{a_0\pi\eta}(p^2) G_{a_0\gamma^*\gamma}^{(K)}(p^2, Q^2). \quad (34)$$

We use the scalar meson propagator $D_S(p^2)$ in the form [24]

$$D_S^{-1}(p^2) = p^2 - M_S^2 + M_S \Im m \left(\tilde{\Gamma}_{S, tot}(M_S^2) \right) + i\sqrt{p^2} \tilde{\Gamma}_{S, tot}(p^2) \quad (35)$$

with

$$\tilde{\Gamma}_{tot, S}(p^2) = \tilde{\Gamma}_{S \rightarrow \pi\pi}(p^2) + \tilde{\Gamma}_{S \rightarrow K\bar{K}}(p^2), \quad S = f_0, \sigma$$

$$\tilde{\Gamma}_{tot, a_0}(p^2) = \tilde{\Gamma}_{a_0 \rightarrow \pi\eta}(p^2) + \tilde{\Gamma}_{a_0 \rightarrow K\bar{K}}(p^2). \quad (36)$$

Contributions of heavy particles to the total widths, e.g., $\Gamma_{f_0 \rightarrow \eta\eta}(p^2)$, are neglected. Modified widths $\tilde{\Gamma}$ in the above

Table 2. Effective couplings for scalar mesons [24] (to be used with vertices of Fig. 3). Model parameters are c_d and c_m ; the scalar octet-singlet mixing angle θ is defined in Eq. (A4); η' couplings are omitted; singlet couplings \tilde{c}_d and \tilde{c}_m are related to c_d and c_m in the large- N_c approximation. Notice that the entries relevant to the η meson correct the results of Table 9 in Ref. [12].

$g_{f\pi\pi}$	$= -2c_m m_\pi^2 (2 \cos \theta - \sqrt{2} \sin \theta) / \sqrt{3},$
$g_{f\eta\eta}$	$= -c_m (2(C_s^2(2m_K^2 - m_\pi^2) + C_q^2 m_\pi^2) \cos \theta$ $+ \sqrt{2}(C_s^2(4m_K^2 - 2m_\pi^2) - C_q^2 m_\pi^2) \sin \theta) / \sqrt{3},$
g_{fKK}	$= -c_m m_K^2 (4 \cos \theta + \sqrt{2} \sin \theta) / \sqrt{3}.$
$\hat{g}_{f\pi\pi}$	$= 2c_d (2 \cos \theta - \sqrt{2} \sin \theta) / \sqrt{3},$
$\hat{g}_{f\eta\eta}$	$= c_d (2(C_q^2 + C_s^2) \cos \theta$ $- \sqrt{2}(C_q^2 - 2C_s^2) \sin \theta) / \sqrt{3},$
\hat{g}_{fKK}	$= c_d (4 \cos \theta + \sqrt{2} \sin \theta) / \sqrt{3}.$
$g_{\sigma\pi\pi}$	$= -2c_m m_\pi^2 (\sqrt{2} \cos \theta + 2 \sin \theta) / \sqrt{3},$
$g_{\sigma\eta\eta}$	$= -c_m (-\sqrt{2}(C_s^2(4m_K^2 - 2m_\pi^2) - C_q^2 m_\pi^2) \cos \theta$ $+ 2(C_s^2(2m_K^2 - m_\pi^2) + C_q^2 m_\pi^2) \sin \theta) / \sqrt{3},$
$g_{\sigma KK}$	$= -c_m m_K^2 (-\sqrt{2} \cos \theta + 4 \sin \theta) / \sqrt{3}.$
$\hat{g}_{\sigma\pi\pi}$	$= 2c_d (\sqrt{2} \cos \theta + 2 \sin \theta) / \sqrt{3},$
$\hat{g}_{\sigma\eta\eta}$	$= c_d (\sqrt{2}(C_q^2 - 2C_s^2) \cos \theta$ $+ 2(C_q^2 + C_s^2) \sin \theta) / \sqrt{3},$
$\hat{g}_{\sigma KK}$	$= c_d (-\sqrt{2} \cos \theta + 4 \sin \theta) / \sqrt{3}.$
g_{aKK}	$= -\sqrt{2} c_m m_K^2,$
$g_{a\pi\eta}$	$= -2\sqrt{2} C_q c_m m_\pi^2,$
\hat{g}_{aKK}	$= \sqrt{2} c_d,$
$\hat{g}_{a\pi\eta}$	$= 2\sqrt{2} C_q c_d.$
$g_{f\pi\eta}$	$= \hat{g}_{f\pi\eta} = g_{\sigma\pi\eta} = \hat{g}_{\sigma\pi\eta} = 0,$
$g_{a\pi\pi}$	$= \hat{g}_{a\pi\pi} = g_{a\eta\eta} = \hat{g}_{a\eta\eta} = 0.$
$g_{S\gamma\pi\pi}$	$= -i\hat{g}_{S\pi\pi},$
$g_{S\gamma\eta\eta}$	$= -i\hat{g}_{S\eta\eta},$
$g_{S\gamma KK}$	$= -i\hat{g}_{S KK},$
$g_{S\gamma\pi\eta}$	$= \hat{g}_{S\pi\eta},$
$g_{S\gamma\eta\pi}$	$= \hat{g}_{S\eta\pi},$
$g_{S\gamma\pi K}$	$= \hat{g}_{S\pi K},$
$g_{S\gamma K\pi}$	$= \hat{g}_{S K\pi}.$

expressions are defined similarly to the tree-level decay widths given in Appendix B, see Eqs. (B10), but the analytic continuation is used:

$$\sqrt{f(p^2)} = e^{i \text{Arg}(f(p^2)) / 2} \sqrt{|f(p^2)|}, \quad (37)$$

see Ref. [24].

By construction, the functions f_1 in (33), (34) are of the chiral order $\mathcal{O}(p^6)$: the diagrams of Fig. 4 are $\mathcal{O}(p^4)$ and SPP transition is $\mathcal{O}(p^2)$.

4 Vector contribution

For $\gamma^* \rightarrow (\dots) \rightarrow \pi^0\pi^0\gamma$ the vector contribution mechanisms are listed in Table 3 and the corresponding diagrams are shown in Fig. 5.

For the odd-intrinsic-parity vector-vector-pseudoscalar and vector-photon-pseudoscalar interactions we use the chiral Lagrangian in the vector formulation for spin-1 fields. As shown in [27], the use of vector formulation for

1^- fields ensures the correct behavior of Green functions to order $\mathcal{O}(p^6)$, while the tensor formulation would require additional local terms (see also discussion in the Appendix F of [15]). We choose Lagrangians of Ref. [27,28], that are $\mathcal{O}(p^2)$ and $\mathcal{O}(p^3)$, for construction of the vector γVP and double-vector VVP contribution to f_i . General Lagrangian terms are given in Appendix A.

Assuming exact $SU(3)$ case, the γV interaction can be written as

$$\mathcal{L}_{\gamma V} = -e f_V \partial^\mu B^\nu (\tilde{\rho}_{\mu\nu}^0 + \frac{1}{3} \tilde{\omega}_{\mu\nu} - \frac{\sqrt{2}}{3} \tilde{\phi}_{\mu\nu}) \quad (38)$$

with $\tilde{V}_{\mu\nu} \equiv \partial_\mu V_\nu - \partial_\nu V_\mu$ and $f_V = F_V / M_\rho$ is the coupling for the vector representation of the spin-1 fields [25].

The interactions of vector mesons in the odd-intrinsic-parity sector read

$$\mathcal{L}_{V\gamma P} = -\frac{4\sqrt{2}eh_V}{3f_\pi} \epsilon_{\mu\nu\alpha\beta} \partial^\alpha B^\beta \left[(\rho^{0\mu} + 3\omega^\mu + 3\epsilon_{\omega\phi}\phi^\mu) \partial^\nu \pi^0 \right. \\ \left. + [(3\rho^{0\mu} + \omega^\mu)C_q + 2\phi^\mu C_s] \partial^\nu \eta \right], \quad (39)$$

$$\mathcal{L}_{VVP} = -\frac{4\sigma_V}{f_\pi} \epsilon_{\mu\nu\alpha\beta} \left[\pi^0 \partial^\mu \omega^\nu \partial^\alpha \rho^{0\beta} \right. \\ \left. + \pi^0 \epsilon_{\omega\phi} \partial^\mu \phi^\nu \partial^\alpha \rho^{0\beta} + \pi^0 \epsilon' \partial^\mu \omega^\nu \partial^\alpha \phi^\beta \right. \\ \left. + \eta [(\partial^\mu \rho^{0\nu} \partial^\alpha \rho^{0\beta} + \partial^\mu \omega^\nu \partial^\alpha \omega^\beta) \frac{1}{2} C_q \right. \\ \left. - \partial^\mu \phi^\nu \partial^\alpha \phi^\beta \frac{1}{\sqrt{2}} C_s + \epsilon_{\omega\phi} \partial^\mu \phi^\nu \partial^\alpha \omega^\beta (C_q + C_s) \right], \quad (40)$$

where $\epsilon_{\mu\nu\alpha\beta}$ is the totally antisymmetric Levi-Civita tensor. As before, we omit the η' meson.

As it is also seen from (39) and (40), the transitions $\gamma\phi\pi^0$, $\phi\rho^0\pi^0$ and $\phi\omega\eta$ are related to a small parameter $\epsilon_{\omega\phi}$, responsible for the $u\bar{u} + d\bar{d}$ component in the physical ϕ meson. The parameter ϵ' is responsible for the G-parity-violating $\phi\omega\pi^0$ vertex, caused by isospin breaking. The coupling constants f_V , h_V and θ_V are model parameters. Numerical values for all parameters are given in Appendix B.

Due to a similar structure of the $\mathcal{L}_{V P \gamma}$ and $\mathcal{L}_{V V P}$ interactions, the processes $\gamma^* \rightarrow VP_{1,2} \rightarrow P_1 P_2 \gamma$ (one-vector-meson exchange) and $\gamma^* \rightarrow V_a \rightarrow V_b P_{1,2} \rightarrow P_1 P_2 \gamma$ (double-vector-meson exchange) can be described together. For this purpose it is convenient to introduce the form factors $F_{\gamma^* VP}(Q^2)$ which describe the transitions $\gamma^*(Q^2) \rightarrow VP$ including both these mechanisms. Of course, the vector resonance enters off-mass-shell.

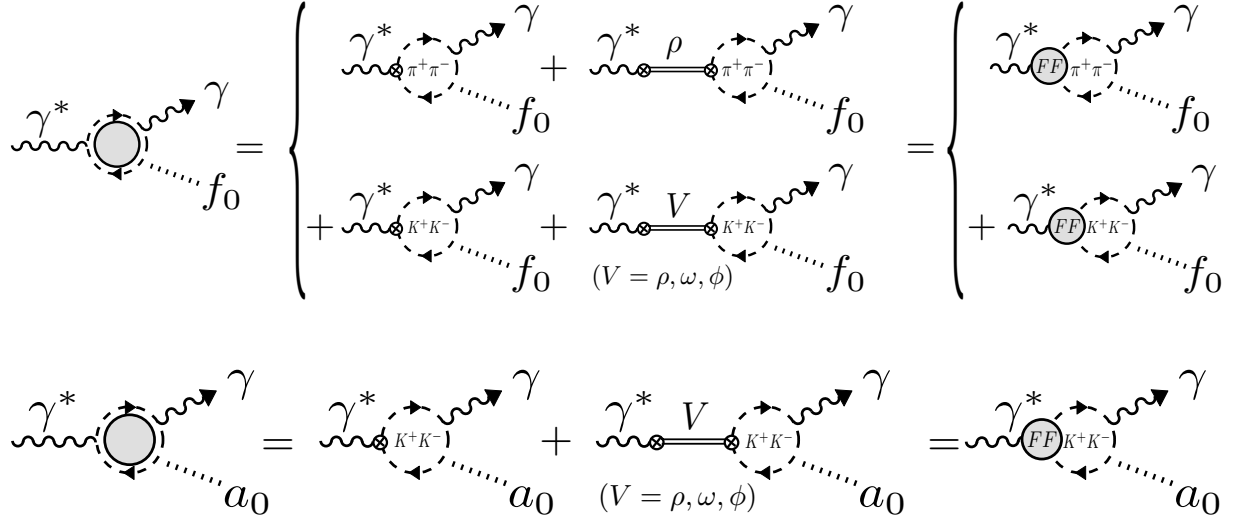


Figure 4. Scheme for the $\gamma^*\gamma f_0$ and $\gamma^*\gamma\sigma$ (top) and $\gamma^*\gamma a_0$ (bottom) transition. Each “loop blob” corresponds to a set of diagrams following from the Lagrangian, as explicitly shown in [12]

For the $\gamma^* \rightarrow V\pi^0$ transition we obtain

$$\begin{aligned}
F_{\gamma^*\rho\pi}(Q^2) &= \frac{4}{3f_\pi} [\sqrt{2}h_V - \sigma_V f_V Q^2 D_\omega(Q^2) \\
&\quad + \varepsilon_{\omega\phi} \sqrt{2}\sigma_V f_V Q^2 D_\phi(Q^2)], \\
F_{\gamma^*\omega\pi}(Q^2) &= \frac{4}{f_\pi} [\sqrt{2}h_V - \sigma_V f_V Q^2 D_\rho(Q^2) \\
&\quad + \varepsilon' \frac{\sqrt{2}}{3} \sigma_V f_V Q^2 D_\phi(Q^2)], \\
F_{\gamma^*\phi\pi}(Q^2) &= \varepsilon_{\omega\phi} \frac{4}{f_\pi} [\sqrt{2}h_V - \sigma_V f_V Q^2 D_\rho(Q^2)].
\end{aligned} \tag{41}$$

The vector meson $V = \rho, \omega, \phi$ propagators are

$$D_V(Q^2) = [Q^2 - M_V^2 + i\sqrt{Q^2}\Gamma_{tot,V}(Q^2)]^{-1}. \tag{42}$$

with an energy-dependent width for the ρ meson

$$\begin{aligned}
\Gamma_{tot,\rho}(Q^2) &= \frac{G_V^2 M_\rho^2}{48\pi f_\pi^4 Q^2} \left[(Q^2 - 4m_\pi^2)^{3/2} \theta(Q^2 - 4m_\pi^2) \right. \\
&\quad \left. + \frac{1}{2} (Q^2 - 4m_K^2)^{3/2} \theta(Q^2 - 4m_K^2) \right]
\end{aligned} \tag{43}$$

and the constant widths for the ω and ϕ mesons.

In terms of these FF's we find the contribution to the functions f_i (see Eq. (7)) coming from the processes (3).

For the $\pi^0\pi^0\gamma$ final state one obtains:

$$\begin{aligned}
f_1^V &= -\frac{1}{4} \sum_{V=\rho,\omega} F_{\gamma^*V\pi}(Q^2) F_{\gamma^*V\pi}(0) \\
&\quad \times [(k \cdot Q + l^2)(D_V(R_+^2) + D_V(R_-^2)) \\
&\quad + 2k \cdot l (D_V(R_+^2) - D_V(R_-^2))], \\
f_2^V &= \frac{1}{4} \sum_{V=\rho,\omega} F_{\gamma^*V\pi}(Q^2) F_{\gamma^*V\pi}(0) [D_V(R_+^2) + D_V(R_-^2)], \\
f_3^V &= -\frac{1}{4} \sum_{V=\rho,\omega} F_{\gamma^*V\pi}(Q^2) F_{\gamma^*V\pi}(0) [D_V(R_+^2) - D_V(R_-^2)],
\end{aligned} \tag{44}$$

where the contribution proportional to $F_{\gamma^*\phi\pi}(Q^2) F_{\gamma^*\phi\pi}(0) \propto \varepsilon_{\omega\phi}^2$ has been neglected. The momenta are defined as

$$R_\pm^2 = (1/4)(Q^2 + l^2 + 2k \cdot Q \pm 2(k \cdot l + Q \cdot l)), \tag{45}$$

or equivalently $R_+^2 = (k + p_1)^2$ and $R_-^2 = (k + p_2)^2$.

Similarly, for the $\gamma^* \rightarrow V\eta$ transition we obtain FF's

$$\begin{aligned}
F_{\gamma^*\rho\eta}(Q^2) &= C_q F_{\gamma^*\omega\pi}(Q^2), \\
F_{\gamma^*\omega\eta}(Q^2) &= C_q F_{\gamma^*\rho\pi}(Q^2), \\
F_{\gamma^*\phi\eta}(Q^2) &= 2 C_s \frac{4}{3f_\pi} [\sqrt{2}h_V - \sigma_V f_V Q^2 D_\phi(Q^2) \\
&\quad - \varepsilon_{\omega\phi} (C_q + C_s) \frac{4}{3f_\pi} \sigma_V f_V Q^2 D_\omega(Q^2)].
\end{aligned} \tag{46}$$

Correspondingly, the contribution to the functions f_i for the $\pi^0\eta\gamma$ final state is

$$\begin{aligned}
f_1^V &= -\frac{1}{4} \sum_{V=\rho,\omega,\phi} \left\{ F_{\gamma^*V\pi}(0) F_{\gamma^*V\eta}(Q^2) \right. \\
&\quad \times [(k \cdot Q + l^2) D_V(R_+^2) + 2k \cdot l D_V(R_+^2)] \\
&\quad + F_{\gamma^*V\eta}(0) F_{\gamma^*V\pi}(Q^2) \\
&\quad \left. \times [(k \cdot Q + l^2) D_V(R_-^2) - 2k \cdot l D_V(R_-^2)] \right\}, \\
f_2^V &= \frac{1}{4} \sum_{V=\rho,\omega,\phi} \left\{ F_{\gamma^*V\pi}(0) F_{\gamma^*V\eta}(Q^2) D_V(R_+^2) \right. \\
&\quad \left. + F_{\gamma^*V\eta}(0) F_{\gamma^*V\pi}(Q^2) D_V(R_-^2) \right\}, \\
f_3^V &= -\frac{1}{4} \sum_{V=\rho,\omega,\phi} \left\{ F_{\gamma^*V\pi}(0) F_{\gamma^*V\eta}(Q^2) D_V(R_+^2) \right. \\
&\quad \left. - F_{\gamma^*V\eta}(0) F_{\gamma^*V\pi}(Q^2) D_V(R_-^2) \right\}. \tag{47}
\end{aligned}$$

5 Numerical results

In this section we present the numerical results obtained in our framework. The model-dependent ingredients, namely, the functions $f_{1,2,3}$ are given in Sections 3 and 4.

The values of the model parameters, which we used in our numerical results, are listed in Appendix B. The masses of vector and pseudoscalar mesons are taken from [1]. The coupling of vector mesons to a pseudoscalar and photon h_V is estimated from the tree-level decay width. The scalar meson couplings and mass parameters were found from the fit [24].

5.1 Scalar mesons and ϕ radiative decay

As we discussed in this paper, in e^+e^- annihilation to $\pi^0\pi^0\gamma$ and $\pi^0\eta\gamma$ both scalar (2) and vector decays (3) contribute to the observed events. The KLOE Collaboration has reported data on the invariant mass distributions [2,4] at $\sqrt{s} = M_\phi$, in which the vector meson contribution has been subtracted. In [24] we performed a combined fit of $dB(\phi \rightarrow a_0\gamma \rightarrow \pi^0\eta\gamma)/d\sqrt{p^2}$ and $dB(\phi \rightarrow (f_0, \sigma)\gamma \rightarrow \pi^0\pi^0\gamma)/d\sqrt{p^2}$ to the KLOE 2002 data [2,4], considering only scalar meson contributions. We have found the inclusion of the σ meson into the framework important, and have fixed the numerical values of scalar meson couplings and mass parameters within the model, for more detail see [24]. In Fig. 6 we show our model results for $dB(\phi \rightarrow S\gamma \rightarrow P_1P_2\gamma)/d\sqrt{p^2}$, eq. (19), at $\sqrt{s} = M_\phi$. In this and subsequent plots we use the notation $m_{\pi^0\pi^0}$ and $m_{\eta\pi^0}$ for $\sqrt{p^2}$. Note that only the scalar meson contribution to the $P_1P_2\gamma$ final state is plotted in this Figure. The plot for the $\pi^0\pi^0\gamma$ final state shows a rather good fit [24] to the KLOE 2002 data [4], where both f_0 and σ are taken into account.

In 2009 the new KLOE data [3] on the $\pi^0\eta\gamma$ channel appeared. A comparison of the model prediction for

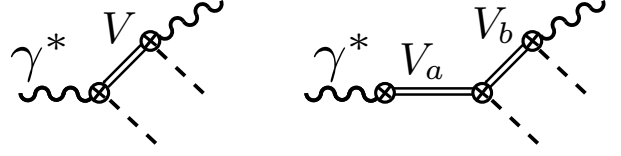


Figure 5. The vector, $\gamma^* \rightarrow VP_1 \rightarrow P_1P_2\gamma$, and double vector, $\gamma^* \rightarrow V_a \rightarrow V_bP_1 \rightarrow P_1P_2\gamma$, contributions

Table 3. Mechanisms of the vector contribution. Notice that some of the channels, suppressed due to small parameters, can be enhanced in the vicinity of the corresponding resonance (e.g. $\gamma^* \rightarrow \phi \rightarrow \omega\pi^0$, see the text)

	Dominant	Suppressed
in $\gamma^* \rightarrow (\dots) \rightarrow \pi^0\pi^0\gamma$:		
1-vector	$(\rho^0\pi^0), (\omega\pi^0)$	$(\phi\pi^0)$
2-vector	$(\omega \rightarrow \rho^0\pi^0), (\rho^0 \rightarrow \omega\pi^0)$	$(\phi \rightarrow \rho^0\pi^0), (\phi \rightarrow \omega\pi^0)$ $(\rho^0 \rightarrow \phi\pi^0)$
in $\gamma^* \rightarrow (\dots) \rightarrow \pi^0\eta\gamma$:		
1-vector	$(\rho\pi^0), (\omega\pi^0)$ $(\rho\eta), (\omega\eta)$	$(\phi\pi^0)$ $(\phi\eta)$
2-vector	$(\rho \rightarrow \omega\pi^0), (\omega \rightarrow \rho\pi^0)$ $(\rho \rightarrow \rho\eta), (\omega \rightarrow \omega\eta)$	$(\rho \rightarrow \phi\pi^0), (\phi \rightarrow \rho\pi^0)$ $(\phi \rightarrow \phi\eta), (\phi \rightarrow \omega\eta)$

$\phi \rightarrow a_0\gamma \rightarrow \pi^0\eta\gamma$ with these new data is also shown in Fig. 6 (bottom). We leave a refined fit of these new data for the future. Notice, if one adds vector contributions to $\sigma(e^+e^- \rightarrow \eta\pi^0\gamma)$ according to Table 3, then the shape of the invariant mass distribution, calculated from eq. (19), changes: cf. Fig. 6 (bottom) and Fig. 7. It turns out that the 2009 KLOE data [3] are better described by the total contribution rather than by the scalar part alone. Note that in Refs. [3,8] it was claimed that the $\phi \rightarrow \pi^0\eta\gamma$ decay is dominated by the $\phi \rightarrow a_0\gamma$ mechanism and the vector contribution is very small: $B(e^+e^- \rightarrow VP \rightarrow \eta\pi^0\gamma) \lesssim 10^{-6}$.

5.2 The $\gamma^* \rightarrow \rho \rightarrow \omega\pi$ and $\gamma^* \rightarrow \phi \rightarrow \omega\pi$ contribution

For the moment, to follow KLOE analysis [5] we neglect the G -parity-violating vertex $\phi\omega\pi^0$, i.e., we set $\varepsilon' = 0$. For illustration we introduce the constant $C_{\omega\pi}^\rho$ [5,18]. This constant can be obtained in terms of form factors (41)

$$\frac{C_{\omega\pi}^\rho(s)}{16\pi\alpha} = -\frac{1}{4} F_{\gamma^*\omega\pi}(s) F_{\gamma^*\omega\pi}(0), \tag{48}$$

leading to

$$\begin{aligned}
C_{\omega\pi}^\rho &= -16\pi\alpha \frac{4\sqrt{2}h_V}{f_\pi^2} \left(\sqrt{2}h_V - \sigma_V f_V s D_\rho(s) \right) \\
&\approx (0.597 - 0.542 i) \text{ GeV}^{-2} \tag{49}
\end{aligned}$$

at $\sqrt{s} = M_\phi$. The KLOE result [5] for the same constant is $C_{\omega\pi}^\rho = 0.850 \text{ GeV}^{-2}$ ($\sqrt{s} = M_\phi$). Thus our prediction for

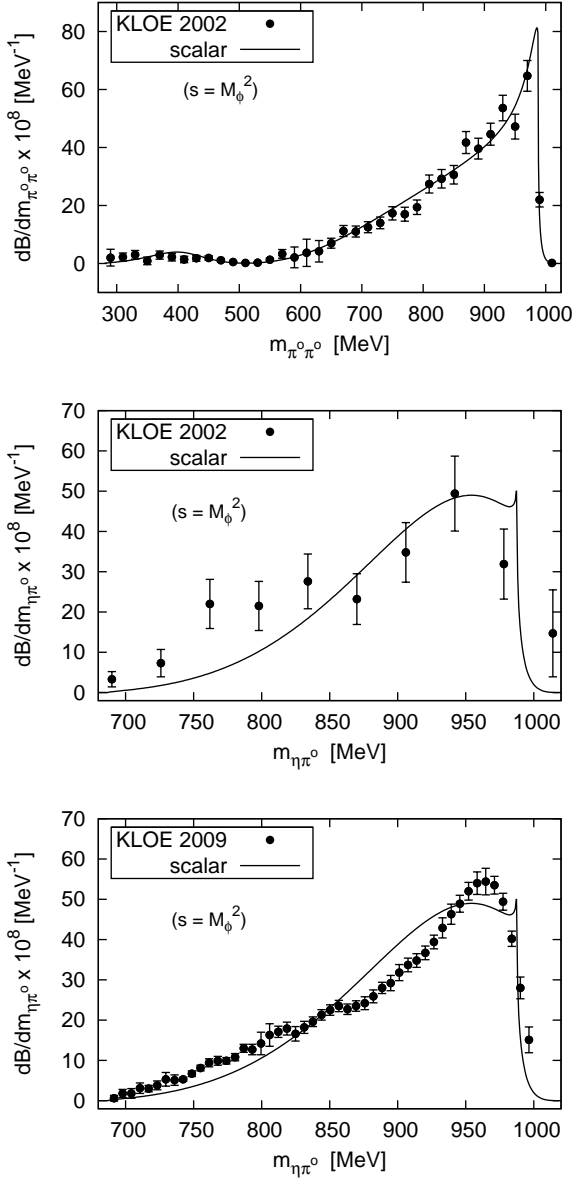


Figure 6. Invariant mass distributions in the e^+e^- annihilation to $\pi^0\pi^0\gamma$ (top panel) and $\pi^0\eta\gamma$ (middle and bottom panel) for $\sqrt{s} = M_\phi$. Data are from [4] (top), [2] (middle) and [3] (bottom)

the absolute value, $|C_{\omega\pi}^\rho| = 0.751 \text{ GeV}^{-2}$, which includes only the $\gamma^*(\rightarrow \rho) \rightarrow \omega\pi$ mechanism, is smaller than that of KLOE by about 15%.

This difference can be attributed to the $\rho' = \rho(1450)$ meson which is not included in the present calculation. To estimate the role of the ρ' in the constant $C_{\omega\pi}^\rho$, we follow

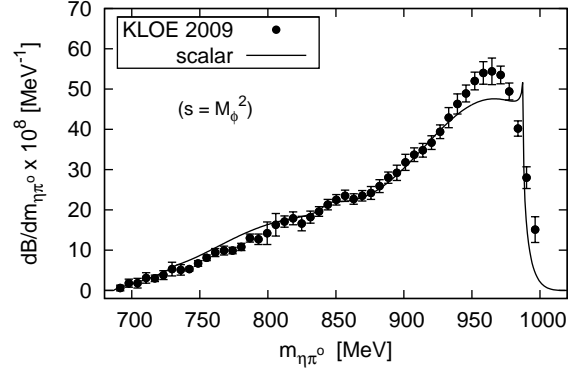


Figure 7. Invariant mass distributions in the e^+e^- annihilation to $\pi^0\eta\gamma$ for $\sqrt{s} = M_\phi$, where the total contribution (vector and scalar) is taken into account (cf. Fig. 6 (bottom)). Data are from [3].

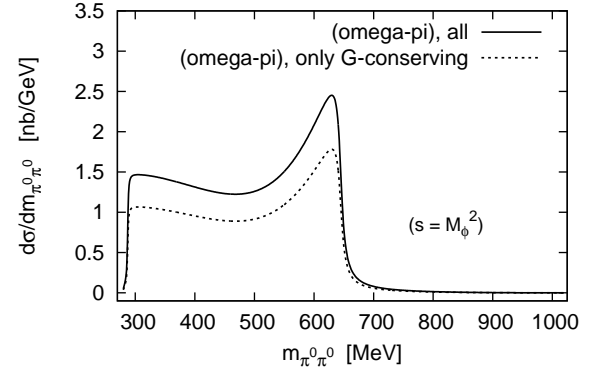


Figure 8. Partial differential cross section of e^+e^- annihilation to $\pi^0\pi^0\gamma$ for $\sqrt{s} = M_\phi$ due to the $\gamma^* \rightarrow \rho \rightarrow \omega\pi$ mechanism compared to $\gamma^* \rightarrow (\rho, \phi) \rightarrow \omega\pi$

Ref. [29] (Eqs. (32), (33)):

$$C_{\omega\pi}^\rho = -16\pi\alpha \frac{4\sqrt{2}h_V}{f_\pi^2} (\sqrt{2}h_V - \sigma_V f_V \frac{s}{1+\beta_{\rho'}} (D_\rho(s) + \beta_{\rho'} D_{\rho'}(s))) \approx (1.06 - 0.69 i) \text{ GeV}^{-2} \quad (50)$$

for $\beta_{\rho'} = -0.25$, $M_{\rho'} = 1.465 \text{ GeV}$, $\Gamma_{\rho'}(M_{\rho'}^2) = 400 \text{ MeV}$ and obtain $|C_{\omega\pi}^\rho| = 1.27 \text{ GeV}^{-2}$.

Next we turn on the parameter ε' responsible for the G -parity-violating $\phi\pi\omega$ vertex and check how the $C_{\omega\pi}^\rho$ value changes. Omitting ρ' we have

$$C_{\omega\pi}^\rho = -16\pi\alpha \frac{4\sqrt{2}h_V}{f_\pi^2} (\sqrt{2}h_V - \sigma_V f_V s D_\rho(s) + \frac{\sqrt{2}}{3} \sigma_V f_V s \varepsilon' D_\phi(s)) \approx (0.52 - 0.72 i) \text{ GeV}^{-2} \quad (51)$$

and obtain $|C_{\omega\pi}^\rho| = 0.892 \text{ GeV}^{-2}$. While making this estimation the value $\varepsilon' = -0.0026$ has been chosen¹. Apparently, the present model with the lowest nonet of vector mesons, supplemented with the G -parity-violating effect, allows one to obtain the value for $C_{\omega\pi}^\rho$ close to the KLOE value 0.850 GeV^{-2} . Influence of the ε' parameter on the cross section is presented in Fig. 8.

Therefore, the difference between the $C_{\omega\pi}^\rho$ value originating from the $\gamma^*(\rightarrow\rho)\rightarrow\omega\pi$ mechanism, and the value measured by KLOE may be explained by the ρ' meson and/or G -parity-violating contribution. To clarify further this issue, an analysis of data at $s = 1 \text{ GeV}^2$ will be essential².

5.3 The $\gamma^* \rightarrow \phi \rightarrow \rho\pi$ and $\gamma^* \rightarrow \omega \rightarrow \rho\pi$

In a similar manner one can define $C_{\rho\pi}(s)$:

$$\begin{aligned} -16\pi\alpha\frac{1}{4}F_{\gamma^*\rho\pi}(s)F_{\gamma^*\rho\pi}(0) &= C_{\rho\pi}(s) \\ &= C_{\rho\pi}^{res}D_\phi(s) + C_{\rho\pi}^\omega, \end{aligned} \quad (52)$$

where

$$\begin{aligned} C_{\rho\pi}^\omega &= -16\pi\alpha\frac{4\sqrt{2}h_V}{9f_\pi^2}(\sqrt{2}h_V - \sigma_V f_V s D_\omega(s)) \\ &\approx (0.091 - 0.002i) \text{ GeV}^{-2} \end{aligned} \quad (53)$$

and

$$\begin{aligned} C_{\rho\pi}^{res} &= -16\pi\alpha\frac{4\sqrt{2}h_V}{9f_\pi^2}\sqrt{2}\sigma_V\varepsilon_{\omega\phi}f_Vs \\ &\approx -0.0052. \end{aligned} \quad (54)$$

The KLOE values for these constants are $C_{\rho\pi}^{res} \approx -0.0057$ and $C_{\rho\pi}^\omega = 0.26 \text{ GeV}^{-2}$. However, in the experiment, they are entangled and one has to compare the total contributions. Using the values (53) and (54) we have $|C_{\rho\pi}(M_\phi^2)| \approx 1.2$, which is in a reasonable agreement with KLOE fit $|C_{\rho\pi}(M_\phi^2)| \approx 1.3$.

5.4 Full model prediction for the cross section

Interference of leading vector resonance contributions ($\rho\pi$) and ($\omega\pi$) is presented in Fig. 9. One can see a destructive interference.

The interplay of the scalar (2) and vector decay (3) contributions to $d\sigma/d\sqrt{p^2}$ is shown in Fig. 10 (for $\sqrt{s} = M_\phi$). One observes a complicated interference between vector and scalar contributions. We see that in the case of the $\pi^0\pi^0\gamma$ final state the vector contribution has the same

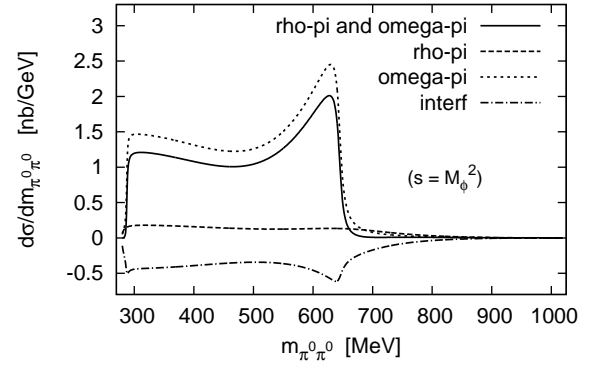


Figure 9. Vector and double-vector decay contributions to $d\sigma/d\sqrt{p^2}$ of $e^+e^- \rightarrow \pi^0\pi^0\gamma$ at $\sqrt{s} = M_\phi$ in the approximation $\varepsilon_{\omega\phi} = 0.058$, $\varepsilon' = -0.0026$. The $(\phi\pi)$ channel is negligible and not shown in the plot

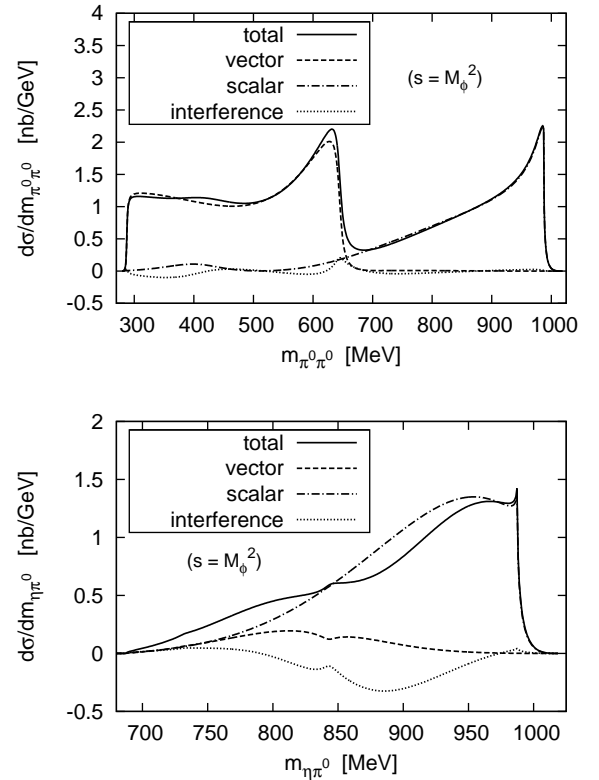


Figure 10. Differential cross section $d\sigma/d\sqrt{p^2}$ of the e^+e^- annihilation to $\pi^0\pi^0\gamma$ (top panel) and $\pi^0\eta\gamma$ (bottom panel) for $\sqrt{s} = M_\phi$

¹ Of course the experimental decay width $\phi \rightarrow \omega\pi$ determines only the absolute value of this parameter.

² At $s = 1 \text{ GeV}^2$ the G -parity-violating vertex is suppressed, whereas the ρ' mechanism survives. Therefore, any difference in the values of $C_{\omega\pi}^\rho$ at two energies, $s = 1 \text{ GeV}^2$ and $s = M_\phi^2$, would indicate sizeable G -parity-violating effects.

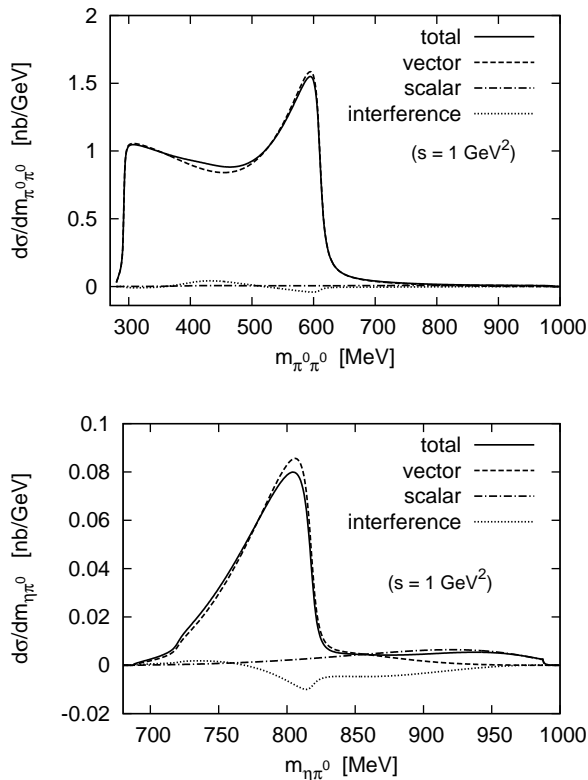


Figure 11. Differential cross section $d\sigma/d\sqrt{p^2}$ of the e^+e^- annihilation to $\pi^0\pi^0\gamma$ (top panel) and $\pi^0\eta\gamma$ (bottom panel) for $\sqrt{s} = 1$ GeV

size as the scalar meson one and is much smaller than the scalar one for the $\pi^0\eta\gamma$ final state.

Notice that there exist the off-peak ($\sqrt{s} = 1$ GeV) data collected by KLOE. The ϕ meson decays get strongly suppressed and the total cross section is determined by the vector contribution only. In order to support the related activity and provide the important model estimates, we include this case into our numerical calculation. The corresponding results are presented in Fig. 11.

6 Conclusions

We presented a general framework for the model-independent decomposition of the differential cross section for the final-state radiation in the reactions $e^+e^- \rightarrow \pi^0\pi^0\gamma$ and $e^+e^- \rightarrow \pi^0\eta\gamma$, for which the ISR contribution is absent and the leading-order cross section is determined solely by the FSR mechanism.

We calculated the explicit form of the functions f_i , which carry the model-dependent information about the processes. Scalar resonance, vector and double vector meson exchange contributions are considered. Notice that all the relative phases are fixed from the Lagrangian of Resonance Chiral Theory. The only exception is the sign of the ε' parameter, which is related to a rare $\phi \rightarrow \omega\pi$ decay.

The Lagrangian is taken at the linear-in-resonance level in the even-intrinsic-parity sector and at the bilinear-in-resonance level in the odd-intrinsic-parity sector. For agreement with data, the $R\chi T$ Lagrangian with the lowest nonet of vector and scalar mesons [20] was extended by including some $SU(3)$ symmetry breaking effects. At the same time, we tried to keep the number of model parameters as small as possible, using additional constraints. The model parameters for the scalar sector were obtained from the fit [24] to the KLOE data [2,4].

As a by-product, we also obtained predictions for various transition form factors: $\gamma^*\gamma S$, SPP , γ^*VP and γ^*PP . These expressions follow directly from the Lagrangian, and the corresponding parameters are fixed to a large extent.

The numerical results for the differential cross section $d\sigma/d\sqrt{p^2}$ are given for two cases: $\sqrt{s} = 1$ GeV and $\sqrt{s} = M_\phi$ and demonstrate an interplay of the scalar and vector decay contributions. The influence of the scalar and vector contributions on the cross section is studied in detail.

The main conclusions of the numerical studies are the following:

- for the $\pi^0\eta\gamma$ final state the vector contribution is much smaller than the scalar one at $\sqrt{s} = M_\phi$ whereas for the $\pi^0\pi^0\gamma$ channel the vector and scalar contributions are of the same size;
- among the vector contributions to the $\pi^0\pi^0\gamma$ channel the leading one comes from the $\gamma^*(\rightarrow (\rho; \phi)) \rightarrow \omega\pi$ mechanism; comparing to the KLOE fit [5] we have concluded that about 85% of this contribution is caused by the ρ intermediate state, and the rest can be explained either by the $\rho(1450)$ or by the G-parity-violating process: $\gamma^* \rightarrow \phi \rightarrow \omega\pi$. New experimental data at $\sqrt{s} = 1$ GeV can help to clarify which of these two mechanisms is responsible for the rest;
- at $\sqrt{s} = 1$ GeV the scalar contribution is suppressed and the total cross section is determined only by the vector contribution both for the $\pi^0\pi^0\gamma$ and $\pi^0\eta\gamma$ channels.

At the end, we would like to emphasize that the developed approach allows one to obtain the cross section and branching fraction close to the experimental results. The main advantage of this approach is a small number of model parameters.

The proposed framework can be implemented in a Monte Carlo generator, for the inspection of the completely differential characteristics of the reaction, and thus is useful for a data analysis and a detailed comparison of various models.

Acknowledgements. We would like to thank Zurab Silagadze for his comments on [17] and for providing us with a copy of [22]. This paper profited from discussions with Henryk Czyż. S.E., A.K. and O.S. acknowledge partial support by the INTAS grant 05-100008-8328 “Higher order effects in e^+e^- annihilation and muon anomalous magnetic moment”. S.E. acknowledges partial support by RFFI grant 09-02-01143. S.I. was supported in part by Research Training Network EU-MRTN-CT-2006-035482 (FLAVIANet). G.P. is grateful to the MIT Center

of Theoretical Physics for hospitality while this work was being written.

Appendix A: Pseudoscalar mesons, scalar multiplet and the $R\chi T$ Lagrangian

In chiral theory, the pseudoscalar mesons π , K , η can be treated as pseudo-Nambu-Goldstone bosons of spontaneous $G = SU(3)_L \times SU(3)_R$ to $H = SU(3)_V$ broken symmetry. The physical states η , η' can be introduced using the scheme with two mixing angles (θ_0, θ_8) , for a review see [30]. The adopted scheme is consistent with chiral theory and takes into account the effects of $U(1)$ axial anomaly and $SU(3)$ flavor breaking ($m_s \gg m_{u,d}$). In our notation [24] the pseudoscalar nonet reads

$$u = \exp \left\{ \frac{i}{\sqrt{2}f_\pi} \begin{pmatrix} \frac{\pi^0 + C_q\eta + C'_q\eta'}{\sqrt{2}} & \pi^+ & \frac{f_\pi}{f_K} K^+ \\ \pi^- & \frac{-\pi^0 + C_q\eta + C'_q\eta'}{\sqrt{2}} & \frac{f_\pi}{f_K} K^0 \\ \frac{f_\pi}{f_K} K^- & \frac{f_\pi}{f_K} \bar{K}^0 & -C_s\eta + C'_s\eta' \end{pmatrix} \right\}, \quad (\text{A1})$$

where

$$\begin{aligned} C_q &\equiv \frac{f_\pi}{\sqrt{3} \cos(\theta_8 - \theta_0)} \left(\frac{1}{f_0} \cos \theta_0 - \frac{1}{f_8} \sqrt{2} \sin \theta_8 \right), \\ C'_q &\equiv \frac{f_\pi}{\sqrt{3} \cos(\theta_8 - \theta_0)} \left(\frac{1}{f_8} \sqrt{2} \cos \theta_8 + \frac{1}{f_0} \sin \theta_0 \right), \\ C_s &\equiv \frac{f_\pi}{\sqrt{3} \cos(\theta_8 - \theta_0)} \left(\frac{1}{f_0} \sqrt{2} \cos \theta_0 + \frac{1}{f_8} \sin \theta_8 \right), \\ C'_s &\equiv \frac{f_\pi}{\sqrt{3} \cos(\theta_8 - \theta_0)} \left(\frac{1}{f_8} \cos \theta_8 - \frac{1}{f_0} \sqrt{2} \sin \theta_0 \right). \end{aligned} \quad (\text{A2})$$

The vielbein field which represents the pseudoscalar mesons is $u_\mu = iu^+ D_\mu u^+$ and $\chi_+ = u^+ \chi u^+ + u \chi u$ is the explicit symmetry-breaking term, $\chi \approx \text{diag}(m_\pi^2, m_\pi^2, 2m_K^2 - m_\pi^2)$ in the isospin symmetry limit.

The electromagnetic field B^μ is included as an external source, $F_{\mu\nu} = \partial_\mu B_\nu - \partial_\nu B_\mu$ is the electromagnetic field tensor. It appears in the chiral covariant derivative, which in our case is reduced to $D_\mu U = \partial_\mu U + ieB_\mu[U, Q]$ and in the tensor $f_+^{\mu\nu} = eF^{\mu\nu}(uQu^+ + u^+Qu)$, where the quark charge matrix $Q = \text{diag}(2/3, -1/3, -1/3)$.

For calculations in the even-intrinsic-parity sector, the leading-order $R\chi T$ Lagrangian for pseudoscalar, scalar, vector mesons and photons was derived by Ecker *et al.* [20]. The spin-1 mesons are described by antisymmetric matrix tensor fields $V^{\mu\nu}$ and this Lagrangian is equivalent to the ChPT Lagrangian at order $\mathcal{O}(p^4)$ (see [20,25] for details). In our application we have somewhat relaxed the rigor of $R\chi T$ and use different masses of resonances ($M_\rho \neq M_\omega \neq M_\phi$ and $M_\sigma \neq M_{a_0} \neq M_{f_0}$) without specifying a pattern of flavor symmetry breaking (cf. Ref. [31]).

Interaction terms for the pseudoscalar and vector mesons read

$$\mathcal{L}_{vector} = \frac{f^2}{4} \langle u_\mu u^\mu + \chi_+ \rangle + \frac{F_V}{2\sqrt{2}} \langle V_{\mu\nu} f_+^{\mu\nu} \rangle + \frac{iG_V}{\sqrt{2}} \langle V_{\mu\nu} u^\mu u^\nu \rangle, \quad (\text{A3})$$

here $\langle \dots \rangle$ stands for the trace in flavor space.

For scalar mesons we assume the nonet symmetry of the interaction terms and multiplet decomposition

$$\begin{cases} a_0 = S_3, \\ f_0 = S_0 \cos \theta - S_8 \sin \theta, \\ \sigma = S_0 \sin \theta + S_8 \cos \theta, \end{cases} \quad (\text{A4})$$

where S_3 is the neutral isospin-one, S_8 is the isospin-zero member of the flavor octet. The angle θ is the octet-singlet mixing parameter, and $\sigma \equiv f_0(600)$. The interaction Lagrangian for scalars takes the form

$$\mathcal{L}_{scalar} = c_d \langle S u_\mu u^\mu \rangle + c_m \langle S \chi_+ \rangle. \quad (\text{A5})$$

There are known problems with a rigorous inclusion of σ and $f_0(980)$ into any $R\chi T$ multiplet [31]. However, there is also a number of successful applications [32,33] of a scheme similar to (A4). In studies of ϕ radiative decays this scheme was also applied in [24,26].

Due to nonet symmetry, the relation for scalar singlet S_0 and octet S^{oct} coupling constants holds, $c_{m,d} S = c_{m,d} (S^{oct} + S_0/\sqrt{3})$. In nomenclature of Ref. [20] this relation implies $\tilde{c}_{m,d} = c_{m,d}/\sqrt{3}$.

In the odd-intrinsic-parity sector the flavor $SU(3)$ symmetric Lagrangian [27,28] reads

$$\begin{aligned} \mathcal{L}_{odd} &= h_V \epsilon_{\mu\nu\alpha\beta} \langle V^\mu (u^\nu f_+^{\alpha\beta} + f_+^{\alpha\beta} u^\nu) \rangle \\ &+ \sigma_V \epsilon_{\mu\nu\alpha\beta} \langle V^\mu (u^\nu \partial^\alpha V^\beta + \partial^\alpha V^\beta u^\nu) \rangle. \end{aligned} \quad (\text{A6})$$

Appendix B: Model parameters

Masses

The following values for the meson masses are used in our numerical calculations [1]: $M_\rho = 775.49$ MeV, $M_\omega = 782.65$ MeV, $M_\phi = 1019.456$ MeV, $m_\pi = m_{\pi^\pm} = 139.57$ MeV, $m_{\pi^0} = 134.98$ MeV, $m_K = 493.68$ MeV, $m_\eta = 547.75$ MeV.

Mixing parameters

The values of the η mixing angles $\theta_0 = -9.2^\circ \pm 1.7^\circ$ and $\theta_8 = -21.2^\circ \pm 1.6^\circ$ are used [35], thus $f_8 = (1.26 \pm 0.04)f_\pi$ and $f_0 = (1.17 \pm 0.03)f_\pi$, where $f_\pi \approx 92.4$ MeV. Thus, one obtains $C_q \approx 0.738$ and $C_s \approx 0.535$.

The $\omega\phi$ mixing is given by one parameter $\varepsilon_{\omega\phi} = 0.058$ [36]. The states of ‘‘ideal mixing’’ $\omega_{id} = (u\bar{u} + d\bar{d})/\sqrt{2}$

and $\phi_{id} = s\bar{s}$ are expressed in terms of the physical ones (mass eigenstates) as

$$\begin{aligned}\omega_{id} &= \omega + \varepsilon_{\omega\phi}\phi, \\ \phi_{id} &= \phi - \varepsilon_{\omega\phi}\omega.\end{aligned}\quad (\text{B1})$$

In order to include a G-parity-violating $\phi\omega\pi^0$ vertex we determine the parameter ε' from the $\phi \rightarrow \omega\pi$ decay width:

$$\Gamma(\phi \rightarrow \omega\pi) = \frac{|g_{\phi\omega\pi}|^2 p_\pi^3}{12\pi}, \quad (\text{B2})$$

where $p_\pi = \sqrt{(M_\phi^2 + m_\pi^2 - M_\omega^2)^2 / (4M_\phi^2) - m_\pi^2}$, the effective coupling in our formalism is $g_{\phi\omega\pi} = 4\sigma_V \varepsilon' / f_\pi$. Using the experimental value for the $\phi \rightarrow \omega\pi$ decay branching ratio $B = (4.4 \pm 0.6) \times 10^{-5}$ [34] and $\sigma_V = 0.34$ one obtains $|\varepsilon'| = 0.0026$.

Couplings in the even-intrinsic-parity sector

The condition $F_V = 2 G_V$ for the model couplings is used in our calculation to make the one-loop amplitude finite [12] without use of counter-terms. This relation has been addressed in [25] in a different context, namely it has been shown that the constraints imposed by the high-energy behavior of the vector and axial-vector FF's lead to it, in addition to the relation $F_V G_V = f_\pi^2$. Note that $F_V = 2 G_V$ also appears in alternative models, e.g., Hidden Local Gauge Symmetry Model and massive Yang-Mills theory for vector mesons, see a discussion in [25]. For numerical calculations we use $G_V = f_\pi / \sqrt{2} = 65.34$ MeV, $F_V = 2 G_V = 130.68$ MeV.

Alternatively, respecting phenomenology, one may fix F_V and G_V by means of fitting the measured partial decay widths of the vector mesons (see, e.g., [20]) at tree level. In particular, for $\rho \rightarrow e^+e^-$ one has

$$\Gamma_{\rho \rightarrow e^+e^-} = \frac{e^4 F_V^2}{12\pi M_\rho} \quad (\text{B3})$$

and for the $\rho \rightarrow \pi\pi$ the tree level width is given by

$$\Gamma_{\rho \rightarrow \pi^+\pi^-} = \frac{G_V^2}{48\pi f_\pi^4} (m_\rho^2 - 4m_\pi^2)^{3/2}. \quad (\text{B4})$$

The experimental data are the following [1]: $\Gamma(\rho \rightarrow \pi^+\pi^-) = 146.2 \pm 0.7$ MeV and $\Gamma_{\rho \rightarrow e^+e^-} = 7.04 \pm 0.06$ keV. Values obtained in this way are $G_V = 65.14 \pm 0.16$ MeV and $F_V = 156.41 \pm 0.67$ MeV. The estimated values support the $F_V \approx 2 G_V$ conjecture.

Couplings in the odd-intrinsic-parity sector

The coupling constant f_V is given by $f_V = F_V / M_\rho \approx 0.17$. The parameter h_V can be fixed from the $V \rightarrow P\gamma$ decay width, in particular, the $\rho \rightarrow \pi\gamma$ width

$$\Gamma(\rho \rightarrow \pi\gamma) = \frac{4\alpha M_\rho^3 h_V^2}{27 f_\pi^2} \left(1 - \frac{m_\pi^2}{M_\rho^2}\right)^3 \quad (\text{B5})$$

leads to $h_V = 0.041 \pm 0.003$.

One can use a special short-distance constraint of R χ T in order to relate σ_V to f_V and h_V . Namely, one can require the form factors (46) to vanish at $Q^2 \rightarrow -\infty$ as expected from QCD. In this connection we refer to [37, 38], where in the framework of R χ T high-energy behavior of three-point Green functions VVP , VAP , AAP has been studied.

At $Q^2 \rightarrow -\infty$ the propagators (42) $D_V(Q^2) \rightarrow 1/Q^2$ and we obtain the following relation (neglecting mixing)

$$\sqrt{2}h_V - \sigma_V f_V = 0. \quad (\text{B6})$$

This constraint reduces the number of independent parameters in the model, in particular, expresses the poorly known parameter σ_V via h_V and f_V , which can be fixed from data. Thus we obtain $\sigma_V \approx 0.34$.

Notice, an additional constraint on the parameters σ_V , h_V and f_V follows from the short-distance behavior of the $\gamma^*\gamma^*\pi^0$ form factor (see a discussion in Ref. [38]):

$$-\frac{N_c}{4\pi^2} + 16\sqrt{2}h_V f_V - 8\sigma_V f_V^2 = 0. \quad (\text{B7})$$

It allows to further reduce the number of independent parameters. For example, one can leave f_V to be the only independent parameter and deduce from (B6) and (B7)

$$\begin{aligned}\sigma_V &= \frac{N_c}{32\pi^2 f_V^2}, \\ h_V &= \frac{N_c}{32\sqrt{2}\pi^2 f_V},\end{aligned}\quad (\text{B8})$$

which results in the numerical values $\sigma_V = 0.329$ and $h_V = 0.0395$ — fairly close to those obtained with the use of Eq. (B5).

In favor of broken flavor $SU(3)$ symmetry, one may introduce separate couplings for each vector meson, i.e. replace f_V by f_ρ, f_ω, f_ϕ , and further h_V by $h_{\gamma\rho\pi}, h_{\gamma\omega\pi}, h_{\gamma\rho\eta}, \dots$ (γVP transition), and also σ_V by $\sigma_{\omega\rho\pi}, \sigma_{\rho\rho\eta}, \dots$

Parameters for scalar mesons

The widths for $a_0 \rightarrow \gamma\gamma$ and $f_0 \rightarrow \gamma\gamma$ decays are expressed in terms of (29)–(30), for example:

$$\Gamma_{a_0 \rightarrow \gamma\gamma} = \frac{e^4 p^4}{64\pi\sqrt{p^2}} |G_{a_0\gamma\gamma}^{(K)}(p^2, 0)|^2. \quad (\text{B9})$$

Table 4. Scalar meson parameters [24]. Couplings and mass parameters are given in MeV.

c_d	c_m	M_{a_0}	M_{f_0}	M_σ	θ
93_{-5}^{+11}	46_{-2}^{+9}	1150_{-23}^{+50}	$986.1_{-0.5}^{+0.4}$	504_{-53}^{+242}	$36^\circ \pm 2^\circ$

The strong decay widths of the scalar mesons in the lowest order (tree level) are

$$\Gamma_{a_0 \rightarrow \pi\eta}(p^2) = \frac{|G_{a_0\pi\eta}(p^2)|^2}{8\pi p^2} \times \sqrt{\frac{(p^2 + m_\pi^2 - m_\eta^2)^2}{4p^2} - m_\pi^2}, \quad (\text{B10})$$

$$\Gamma_{f_0 \rightarrow \pi\pi}(p^2) = \left(1 + \frac{1}{2}\right) \frac{|G_{f_0\pi\pi}(p^2)|^2}{8\pi p^2} \times \sqrt{p^2/4 - m_\pi^2},$$

$$\Gamma_{a_0 \rightarrow K\bar{K}}(p^2) = 2 \frac{|G_{a_0KK}(p^2)|^2}{8\pi p^2} \sqrt{p^2/4 - m_K^2},$$

$$\Gamma_{f_0 \rightarrow K\bar{K}}(p^2) = 2 \frac{|G_{f_0KK}(p^2)|^2}{8\pi p^2} \sqrt{p^2/4 - m_K^2},$$

where p^2 is the invariant mass squared of the scalar meson; see also definition (31), (32). For discussion of momentum-dependent couplings $G_{SPP}(p^2)$ and constant SPP couplings of other models (e.g., [10]) see Ref. [26].

The finite-width effects for scalar resonances are very important and expressions (B9), (B10) do not have physical meaning of decay width, when evaluated at the resonance peak value of p^2 . Nevertheless, in several papers, e.g., [12, 20, 39], the tree-level expressions of a similar form were used to find the model parameters (c_d , c_m and θ) from measured widths. It was observed [24, 26, 40] that the coupling constants could be better determined from fitting the $\pi\pi$ and $\pi\eta$ invariant mass distributions in $e^+e^- \rightarrow \phi \rightarrow \gamma\pi\pi$ and $e^+e^- \rightarrow \phi \rightarrow \gamma\pi\eta$ reactions. The fit results [24] are shown in Table 4 and these values are used in our numerical calculations. Notice that for this fit we used data from [4] ($\pi^0\pi^0\gamma$) and [2] ($\pi^0\eta\gamma$). Recently, a new KLOE result for the latter appeared [3], and we find reasonable agreement with it without refitting, see a discussion in Section 5.

Appendix C: Example of the factorization of the $\gamma^* \rightarrow \gamma f_0 \rightarrow \gamma\pi^0\pi^0$ transition amplitude

In this Appendix we sketch the general structure of the scalar meson contribution f_1^S giving emphasis on the appearance of the electromagnetic form factors of the pseudoscalars in the formulae (33) and (34).

Consider the part of the $M^{\mu\nu}$ amplitude (7) of $\gamma^* \rightarrow \gamma f_0 \rightarrow \gamma\pi^0\pi^0$ with a pion loop transition, $M_{\pi loop}^{\mu\nu}$. Figure 4 is of help and one observes two terms

$$M_{\pi loop}^{\mu\nu} = M_{\gamma \rightarrow \pi loop}^{\mu\nu} + M_{\gamma \rightarrow V \rightarrow \pi loop}^{\mu\nu}, \quad (\text{C1})$$

the former with the contact $\gamma^* \rightarrow \pi^+\pi^-$ coupling and the latter with an intermediate vector resonance. They read

$$M_{\gamma \rightarrow \pi loop}^{\mu\nu} = \frac{-4e^2 i}{(4\pi)^2} \tau_1^{\mu\nu} G_{f_0\pi\pi}(p^2) \frac{2}{m_\pi^2} I\left(\frac{Q^2}{m_\pi^2}, \frac{p^2}{m_\pi^2}\right) \times D_{f_0}(p^2) G_{f_0\pi\pi}(p^2) \quad (\text{C2})$$

$$M_{\gamma \rightarrow V \rightarrow \pi loop}^{\mu\nu} = \frac{-4e^2 i}{(4\pi)^2} \tau_1^{\mu\nu} G_{f_0\pi\pi}(p^2) \frac{2}{m_\pi^2} I\left(\frac{Q^2}{m_\pi^2}, \frac{p^2}{m_\pi^2}\right) \times D_{f_0}(p^2) G_{f_0\pi\pi}(p^2) \times \frac{1}{f_\pi^2} F_V G_V Q^2 D_\rho(Q^2). \quad (\text{C3})$$

The ρ meson propagator $D_\rho(Q^2)$ is given in (42). The form factor $G_{f_0\pi\pi}(p^2)$ is given by (31). The loop integral $I(a, b)$ can be found, e.g., in [11] and [14], and reads

$$I(a, b) = \frac{1}{2(a-b)} - \frac{2}{(a-b)^2} \left[f\left(\frac{1}{b}\right) - f\left(\frac{1}{a}\right) \right] + \frac{a}{(a-b)^2} \left[g\left(\frac{1}{b}\right) - g\left(\frac{1}{a}\right) \right], \quad (\text{C4})$$

with

$$f(x) = \begin{cases} -\left[\arcsin\left(\frac{1}{2\sqrt{x}}\right)\right]^2, & x > \frac{1}{4}, \\ \frac{1}{4} \left[\log \frac{n_+(x)}{n_-(x)} - i\pi\right]^2, & 0 < x < \frac{1}{4}, \\ \left[\log \frac{1+\sqrt{1-4x}}{2\sqrt{-x}}\right]^2, & x < 0, \end{cases}$$

$$g(x) = \begin{cases} \sqrt{4x-1} \arcsin\left(\frac{1}{2\sqrt{x}}\right), & x > \frac{1}{4}, \\ \frac{1}{2} \sqrt{1-4x} \left[\log \frac{n_+(x)}{n_-(x)} - i\pi\right], & 0 < x < \frac{1}{4}, \\ \sqrt{1-4x} \log \frac{1+\sqrt{1-4x}}{2\sqrt{-x}}, & x < 0, \end{cases}$$

$$n_\pm(x) = \frac{1}{2x} (1 \pm \sqrt{1-4x}) \quad (\text{C5})$$

For a reference, we remind the alternative notation of [12]:

$$\Psi(m^2, p^2, Q^2) = (a-b)I(a, b), \quad 1/(Q \cdot k) = 2/(Q^2 - p^2), \quad (\text{C6})$$

with $a = Q^2/m^2$ and $b = p^2/m^2$.

Combining (C2) and (C3), one finds

$$M_{\pi loop}^{\mu\nu} = \frac{-4e^2 i}{(4\pi)^2} \tau_1^{\mu\nu} G_{f_0\pi\pi}(p^2) \frac{2}{m_\pi^2} I\left(\frac{Q^2}{m_\pi^2}, \frac{p^2}{m_\pi^2}\right) \times D_{f_0}(p^2) G_{f_0\pi\pi}(p^2) F_{em}^\pi(Q^2) \equiv -ie^2 \tau_1^{\mu\nu} D_{f_0}(p^2) G_{f_0\pi\pi}(p^2) G_{f_0\gamma^*\gamma}^{(\pi)}(p^2, Q^2),$$

where the two-photon form factor of a scalar meson $G_{f_0\gamma^*\gamma}^{(\pi)}(p^2, Q^2)$ is given in (29). The pion electromagnetic form factor $F_{em}^\pi(Q^2)$ in R χ T is given by

$$F_{em}^\pi(Q^2) = 1 - \frac{F_V G_V}{f_\pi^2} Q^2 D_\rho(Q^2). \quad (\text{C7})$$



Figure 12. The $\mathcal{O}(p^2)$ electromagnetic vertex of a (off-mass-shell) pseudoscalar meson in $R\chi T$. All possible intermediate vector resonances $V = \rho^0, \omega, \phi, \dots$ in general contribute. For real photons only the first term on the r.h.s. is non-zero.

Factorization in the part of the $M^{\mu\nu}$ amplitude (7) with a kaon loop transition, $M_{K\text{ loop}}^{\mu\nu}$, is analogous. The kaon form factor in $R\chi T$ is

$$F_{em}^K(Q^2) = 1 - \frac{F_V G_V}{f_K^2} Q^2 \left(\frac{1}{2} D_\rho(Q^2) + \frac{1}{6} D_\omega(Q^2) + \frac{1}{3} D_\phi(Q^2) \right), \quad (C8)$$

The vector meson $V = \rho, \omega, \phi$ propagators are given by (42). The form factors in form (C7) and (C8) include contributions from the photon–vector transition (vector meson dominance, VMD) and the direct γPP interaction, see Fig. 12. The detailed discussion of two versions of VMD (VMD1 and VMD2) is given in the review [41]. It turns out that the $R\chi T$ corresponds to the VMD1 version.

For discussion of the one-loop modification of the electromagnetic vertex and $R\chi T$ -motivated calculation of the kaon form factor see [42].

References

1. C. Amsler *et al.* (The Review of Particle Physics), *Phys. Lett. B* **667** (2008) 1
2. A. Aloisio *et al.* (KLOE Collaboration), *Phys. Lett. B* **536** (2002) 209
3. F. Ambrosino *et al.* (KLOE Collaboration), *Phys. Lett. B* **681** (2009) 5
4. A. Aloisio *et al.* (KLOE Collaboration), *Phys. Lett. B* **537** (2002) 21
5. F. Ambrosino *et al.* (KLOE Collaboration), *Eur. Phys. J C* **49** (2007) 473
6. F. Ambrosino *et al.* (KLOE Collaboration), *Nucl. Phys. Proc. Suppl.* **186** (2009) 290.
7. R.R. Akhmetshin *et al.* (CMD-2 Collaboration), *Phys. Lett. B* **462** (1999) 380.
8. M.N. Achasov *et al.* (SND Collaboration), *Phys. Lett. B* **479** (2000) 53.
9. M. N. Achasov *et al.* (SND Collaboration), *Phys. Lett. B* **485** (2000) 349
10. N.N. Achasov, V.N. Ivanchenko, *Nucl. Phys. B* **315** (1989) 465
11. F. E. Close, N. Isgur and S. Kumano, *Nucl. Phys. B* **389** (1993) 513
12. S. Ivashyn and A. Y. Korchin, *Eur. Phys. J. C* **54** (2008) 89
13. J. A. Oller, *Nucl. Phys. A* **714** (2003) 161
14. A. Bramon, R. Escribano, J. L. Lucio M, M. Napsuciale and G. Pancheri, *Eur. Phys. J. C* **26** (2002) 253
15. S. Dubinsky, A. Korchin, N. Merenkov, G. Pancheri and O. Shekhovtsova, *Eur. Phys. J. C* **40** (2005) 41
16. G. Isidori, L. Maiani, M. Nicolaci and S. Pacetti, *JHEP* **0605** (2006) 049
17. M.N. Achasov *et al.*, *Nucl. Phys.*, B569, 158-182 (2000)
18. O. Shekhovtsova, G. Venanzoni and G. Pancheri, *Comput. Phys. Commun.* **180** (2009) 1206
19. A. Grzelińska, H. Czyż and A. Wapientnik, *Nucl. Phys. Proc. Suppl.* **189** (2009) 216
20. G. Ecker, J. Gasser, A. Pich, E. de Rafael, *Nucl. Phys. B* **321** (1989) 311
21. D. Drechsel, G. Knochlein, A. Metz and S. Scherer, *Phys. Rev. C* **55** (1997) 424
22. S.I. Eidelman and E.A. Kuraev, Novosibirsk preprint 85-101 (1985)
23. A.B. Arbuzov, O.O. Voskresenskaya and E.A. Kuraev, Dubna preprint JINR-E2-95-430 (1995)
24. S. Ivashyn and A. Korchin, PoS (EFT09) 055 (2009), arXiv:0904.4823 [hep-ph]
25. G. Ecker, J. Gasser, H. Leutwyler, A. Pich, E. de Rafael, *Phys. Lett. B* **223** (1989) 425
26. S. Ivashyn and A. Korchin, *Nucl. Phys. Proc. Suppl.* **181-182** (2008) 189
27. G. Ecker, A. Pich, E. de Rafael, *Phys. Lett. B* **237** 481 (1990)
28. J. Prades, *Z. Phys. C* **63** (1994) 491, *Erratum*, *Eur. Phys. J. C* **11** (1999) 571.
29. D. G. Dumm, P. Roig, A. Pich and J. Portoles, *Phys. Lett. B* **685** (2010) 158
30. T. Feldmann, *Int. J. Mod. Phys. A* **15** (2000) 159
31. V. Cirigliano, G. Ecker, H. Neufeld and A. Pich, *JHEP* **0306** (2003) 012
32. G. t’Hooft, G. Isidori, L. Maiani, A. D. Polosa and V. Riquer, *Phys. Lett. B* **662** (2008) 424
33. D. Black, A. H. Fariborz, F. Sannino and J. Schechter, *Phys. Rev. D* **59** (1999) 074026
34. F. Ambrosino *et al.* (KLOE collaboration), *Phys. Lett. B* **669** (2008) 223
35. T. Feldmann, P. Kroll, B. Stech, *Phys. Rev. D* **58** (1998) 114006
36. S. I. Dolinsky *et al.*, *Phys. Rept.* **202** (1991) 99
37. P.D. Ruiz-Femenia, A. Pich, J. Portoles, *JHEP* **0307** (2003) 003
38. M. Knecht, A. Nyffeler, *Eur. Phys. J. C* **21** (2001) 659
39. Z. H. Guo and J. J. Sanz-Cillero, *Phys. Rev. D* **79** (2009) 096006
40. S. Ivashyn and A. Korchin, *AIP Conf. Proc.* **1030** (2008) 123
41. H.B. O’Connell, B.C. Pearce, A.W. Thomas, A.G. Williams, *Prog. Nucl. Part. Phys.* **39** (1997) 201
42. S. A. Ivashyn and A. Y. Korchin, *Eur. Phys. J. C* **49** (2007) 697